Isospin diffusion observables in heavy-ion reactions

T. X. Liu,* W. G. Lynch, M. B. Tsang, X. D. Liu, R. Shomin, W. P. Tan, G. Verde, A. Wagner,† H. F. Xi,‡ and H. S. Xu§
National Superconducting Cyclotron Laboratory and Department of Physics and Astronomy, Michigan State University, East Lansing, Michigan 48824, USA

B. Davin, Y. Larochelle, and R. T. de Souza
Department of Chemistry and IUCF, Indiana University, Bloomington, Indiana 47405, USA

R. J. Charity and L. G. Sobotka
Department of Chemistry, Washington University, St. Louis, Missouri 63130, USA
(Received 20 September 2006; published 6 September 2007)

Collisions of ^{112}Sn and ^{124}Sn nuclei, which differ in their isospin asymmetry, provide information about the rate of isospin diffusion and equilibration. Although several different probes can provide accurate diffusion measurements, the ratios of the mirror nuclei may be the simplest and most promising one. Ratios of the mass seven mirror nuclei yields are analyzed to show the rapidity, transverse momentum, and impact parameter dependence of isospin diffusion.

DOI: 10.1103/PhysRevC.76.034603 PACS number(s): 25.70.Pq

Many investigations have provided theoretical guidance and experimental constraints on the equation of state of symmetric nuclear matter [1]. Dense macroscopic nuclear systems like neutron stars, however, are neutron rich and require an understanding of the density dependence of the symmetry energy term in the nuclear equation of state [2]. Few constraints on this density dependence exist [3], prompting the development of new techniques [4–7] for its determination. Recently, constraints on the density dependence of the symmetry energy were obtained from measurements of isospin diffusion in peripheral nuclear collisions [6,8]. In this article, we identify a set of experimental observables constructed with yield ratios of mirror nuclei that provide consistent measures of the isospin diffusion and extend those experimental investigations to a wider range of rapidity, transverse momentum, and impact parameter.

In a heavy-ion collision involving a projectile and a target with different proton fractions, Z/A, the symmetry energy tends to propel the system toward isospin equilibrium so that the difference between neutron and proton densities is minimized [7]. The isospin asymmetry $\delta = \frac{N-Z}{A}$ of a projectile-like residue produced in a peripheral collision reflects the exchange of nucleons with the target; significant diffusion rates should lead to residues with larger isospin asymmetries for collisions with neutron-rich targets and smaller isospin asymmetries for collisions with proton-rich targets [6,7].

To isolate the isospin diffusion effects from similar effects caused by pre-equilibrium emission, Coulomb, or sequential decays, relative comparisons involving different targets are important. In recent studies, isospin diffusion has been measured by "comparing" $A + B$ collisions of a neutron-rich (A) nucleus and a proton-rich (B) nucleus to symmetric collisions involving two neutron-rich nuclei ($A + A$) and two proton-rich ($B + B$) nuclei under the same experimental conditions [6]. Nonisospin diffusion effects such as pre-equilibrium emission from a neutron-rich (A) projectile should be approximately the same for asymmetric $A + B$ collisions as for symmetric $A + A$ collisions. Similarly, nonisospin diffusion effects from a proton-rich (B) projectile in $B + A$ collisions and $B + B$ collisions should be the same.

The degree of isospin equilibration can be quantified by rescaling the isospin asymmetry δ of a projectile-like residue from a specific collision according to the isospin transport ratio $R_i(\delta)$ [6,9] given by

$$R_i(\delta) = 2\frac{\delta - (\delta_{A+A} + \delta_{B+B})/2}{\delta_{A+A} - \delta_{B+B}}. \quad (1)$$

In the absence of isospin diffusion, $R_i(\delta_{A+B}) = R_i(\delta_{A+A}) = 1$. Likewise without diffusion, $R_i(\delta_{B+A}) = R_i(\delta_{B+B}) = -1$. However, if isospin equilibrum is achieved for roughly equal sized projectile and target nuclei $R_i(\delta_{\mathrm{A+B}}) = R_i(\delta_{\mathrm{B+A}}) \approx 0$. By focusing on the differences in isospin observables between mixed and symmetric systems, $R_i(\delta)$ largely removes the sensitivity to pre-equilibrium emission and enhances the sensitivity to isospin diffusion.

Ideally, one would like to know the asymmetry of the projectile-like residue immediately after the collision and prior to secondary decay because this is the quantity that is calculated in transport theory [6]. To do this, one can measure an observable X that is linearly dependent on the residue asymmetry, i.e., $X = a \cdot \delta + b$, and construct the corresponding isospin transport ratio $R_i(X)$

$$R_i(X) = 2\frac{X - (X_{A+A} + X_{B+B})/2}{X_{A+A} - X_{B+B}}.$$

*Present address: Department of Radiation Oncology, UC Davis Cancer Center, Sacramento, California 95817, USA.
†Present address: Institut für Strahlenphysik, Forschungszentrum Rossendorf, D-01314 Dresden, Germany.
‡Present address: Benton Associate, Toronto, Ontario, Canada.
§Institute of Modern Physics, CAS, Lanzhou 730000, China.

Then, trivial algebraic substitution provides that $R_i(X) = R_i(\delta)$ and one dispenses with most of the uncertainty associated with determining δ from measurements of X.

The above idea has been adopted to study the isospin diffusion using the isoscaling observable ($X = \alpha$) involving two asymmetric collisions ^{124}Sn+^{112}Sn ($A + B$) and ^{112}Sn+^{124}Sn (B + A) and two symmetric collisions ^{124}Sn+^{124}Sn ($A + A$) and ^{112}Sn+^{112}Sn ($B + B$) [6]. The isoscaling parameter α can be obtained from the isotope yield ratios from two reactions, which are similar in all aspects except in their isospin compositions:

$$R_{21}(N, Z) = Y_2(N, Z)/Y_1(N, Z) = C \exp(\alpha N + \beta Z), \quad (2)$$

where $Y_i(N, Z)$ is the yield of the measured fragments with neutron number N and proton number Z emitted in reaction i ($i = 1, 2$), α, β, and C are obtained by fitting the isotope yield ratios to Eq. (2); α is the neutron isoscaling factor, β is the proton isoscaling factor, and C is the normalization constant.

An expression for the dependence of α for particles evaporated from an excited nucleus of asymmetry δ have been derived in Ref. [10] and an identical expression has been obtained for an equilibrium multifragment decay in Ref. [11]. Using expressions from Refs. [10,11], one obtains the following expressions for α and β that may be applicable to both evaporative and multifragment decays of an excited projectile-like fragment:

$$\alpha = \Delta\mu_n/T = 2C_{\text{sym}}(\Delta\delta)(1 - \bar{\delta})/T, \quad (3)$$

$$\beta = \Delta\mu_p/T = -2C_{\text{sym}}(\Delta\delta)(1 + \bar{\delta})/T, \quad (4)$$

and

$$\alpha - \beta = (\Delta\mu_n - \Delta\mu_p)/T = 4C_{\text{sym}}(\Delta\delta)/T, \quad (5)$$

where, $\Delta\delta = \delta_2 - \delta_1$ and $\bar{\delta} = (\delta_2 + \delta_1)/2$ are the differences and mean of the asymmetries of the emitting source, C_{sym} is the coefficient of the symmetry energy term in the nuclear Gibbs free energy. Equations (3)–(5) imply that $\alpha - \beta$ depends linearly on the asymmetry δ of the systems from which the fragments are emitted. For most systems $\delta \ll 1$, making the dependence of α and β on δ essentially linear as well. Both statistical [10,11] and dynamical calculations [12] are consistent with a linear dependence of α, β, and $\alpha - \beta$ on δ.

Although current statistical models are consistent with this linear behavior, one can imagine the development of other models that may not be linearly dependent on δ. For that reason, experimental demonstrations of the linear dependence of the isoscaling parameters on δ are the ultimate authority regarding this question. In the upper panel of Fig. 1, we compare the values for α, β, and $\alpha - \beta$ obtained at midrapidities for central ^{112}Sn+^{112}Sn ($\delta = 0.107$), ^{112}Sn+^{124}Sn ($\delta = 0.153$), and ^{124}Sn+^{124}Sn ($\delta = 0.194$) collisions as a function of the total asymmetry using the data of Ref. [13]. By construction, $\alpha = \beta = \alpha - \beta = 0$ for the reference ^{112}Sn+^{112}Sn system. To ensure complete mixing of projectile and target nucleons, the data in Fig. 1 were obtained at center-of-mass (c.m.) angles of $70^\circ \leqslant \theta_{\text{c.m.}} \leqslant 110^\circ$. This avoids the possible contributions of projectile nucleons near $\theta_{\text{c.m.}} = 0^\circ$ and target nucleons near $\theta_{\text{c.m.}} = 180^\circ$ that are not strongly scattered by the collision. Consistent with theoretical predictions, the measured trends

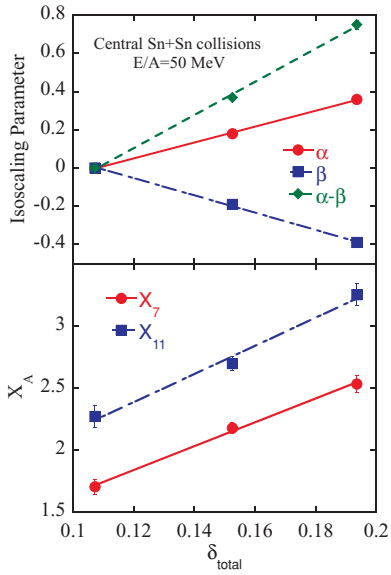

FIG. 1. (Color online) (Upper panel) The circles, squares and diamonds show the experimental data for α, β, and $\alpha - \beta$, respectively, that have been measured for central Sn+Sn collisions. The x axis corresponds to the isospin asymmetry of the combined system. (Lower panel) The solid circles, and solid squares show the experimental data for X_7 and X_{11}, respectively, that has been measured for the same reactions shown in the upper panel.

for α, β, and $\alpha - \beta$ are linear as seen by the data points joined by the solid, dot-dashed, and dashed lines, respectively.

At this point, let us consider the impact of this linear behavior on the subsequent analysis and discussion of isospin transport ratios. When the fragments are produced by the statistical decay of a residue with charge Z_{res}, asymmetry δ, and temperature T, the isoscaling parameters depend sensitively on Z_{res}, δ, and T, i.e., $\alpha = \alpha(Z_{\text{res}}, \delta, T)$ and $\beta = \beta(Z_{\text{res}}, \delta, T)$ [10,11]. (There can be additional dependencies on model assumptions of the statistical theory, such as the level densities and binding energies of the fragments and the time dependence assumed for the disassembly [10–15].) The linear dependence implies that α or β can be written in the form $\alpha(Z_{\text{res}}, \delta, T) = a(Z_{\text{res}}, T) + \delta \cdot b(Z_{\text{res}}, T)$. In the construction of the isospin transport ratio, R_i, the dependencies on $a(Z_{\text{res}}, T)$ and $b(Z_{\text{res}}, T)$ are canceled out algebraicly and R_i depends on δ alone. This does not mean that details of the decay of the residue can be ignored for other observables like the fragment multiplicities, energy spectra, isoscaling parameters, etc. It just means that the effects of residue decay on R_i are so straightforward that one knows the result of taking the residue asymmetries δ, calculating the fragment observables with the residue decay theory, and constructing the theoretical value for $R_i(X)$. The linear behavior ensures that the calculated value for $R_i(X)$ will be equal to the value $R_i(\delta)$ calculated using the residue asymmetry, δ, prior to decay. The data in Fig. 1 clearly establishes the linear dependence of the isoscaling parameters on δ for central collisions, independent of theory. A comparison of the projectile decay in symmetric ^{112}Sn+^{112}Sn, ^{118}Sn+^{118}Sn, and ^{124}Sn+^{124}Sn collisions may provide direct evidence for peripheral collisions. Until such

data are available, the preponderance of theoretical and experimental evidence is for a linear dependence of the isoscaling parameters on δ. We will assume that to be true in the following discussions.

The quantity $\alpha - \beta$ is of particular interest as it arises naturally from the ratios of yields of mirror nuclei $Y(N, Z)$ and $Y(Z, N)$, where $|N - Z| = 1$.

$$r_A = Y_2(N, Z)/Y_1(Z, N) = C \exp(\alpha - \beta) \tag{6}$$

or

$$X_A = \ln(r_A) = \alpha - \beta + \ln(C), \tag{7}$$

where $A = N + Z$ and C is a constant. By using mirror nuclei as discussed below, one avoids mass dependencies in the production mechanism that can make the kinematics of the emitted species mass dependent. The three most widely used pairs of mirror nuclei are (^{3}H, ^{3}He), (^{7}Li, ^{7}Be), and (^{11}B, ^{11}C). Values of X_A obtained for $A = 7$ and 11 from Eq. (7) using the published data of Ref. [13] are shown in the lower panel of Fig. 1. Both X_7 and X_{11} depend linearly on δ.

For the subsequent analyses shown below, we choose X_7 because the yields of ^{7}Li and ^{7}Be are measured with reasonably high statistics. Using X_7, we explore how the isospin diffusion transport ratio varies with rapidity, impact parameter, and transverse momentum. Such explorations require the ability to extract information about the isospin asymmetry from small regions of phase space. It would be more difficult to investigate such issues using the isoscaling parameter α extracted from isotopes of an element. Such isotopes experience the same Coulomb forces from the projectile and target residues, but their collective momentum contributions are proportional to mass, and their thermal momentum contributions are proportional to the square root of their masses. Thus comparisons in small regions of phase space involving fragments of different mass can be a difficult task because the thermal and collective motion influence the momentum distributions of various fragments differently, making it difficult to determine whether an isotopic effect is due to isospin diffusion and not simply kinematics. We find that the use of the isospin transport ratio constructed with the observable X_7 minimizes such kinematic effects. Interestingly, we also find that Coulomb effects, which originate from the differences between the Coulomb repulsion of the ^{7}Li and ^{7}Be fragments from the projectile residue, also largely cancel.

The isotopic distributions produced in ^{112}Sn+^{112}Sn, ^{112}Sn+^{124}Sn, ^{124}Sn+^{112}Sn, and ^{124}Sn+^{124}Sn collisions were measured at the National Superconducting Cyclotron Laboratory at Michigan State University by bombarding ^{112}Sn and ^{124}Sn targets of 5 mg/cm^2 areal density with 50 MeV/nucleon ^{112}Sn and ^{124}Sn beams. Some aspects of these reactions have been published previously [6,13–17]. In the experiment, charged particles were measured with two detection arrays. The multiplicity array consists of 188 plastic scintillator-CsI(Tl) phoswich detectors of the Miniball/Miniwall array [18]. This array provided isotopic resolution for H and He nuclei and elemental resolution for intermediate mass fragments (IMF) with $3 \leqslant Z \leqslant 20$.

In addition to the multiplicity array, the projectile-like residues are detected with a ring counter forward array consists of a double-sided 280-μm-thick annular strip silicon detector backed by an annular array of sixteen 2-cm-thick CsI(Tl) detectors. The annular Si detector is segmented into four quadrants with sixteen 1.5-mm-wide annular strips arranged in circles of increasing radius extending radially from the inner edge of the detector (48-mm diameter) to the outer edge of the detector (96-mm diameter). This provided resolution in the polar angle. The azimuthal angles of the silicon detector were subdivided into 16 azimuthal pads on the opposite side of the detector. The ring counter forward array is centered around the beam axis and covers the polar angles from 2.2° to 4.5°. It provides element resolution for fragments with $3 \leqslant Z \leqslant 55$.

The third array, called the large angle Si strip array (LASSA) [19,20], consists of nine telescopes, each of which comprises one 65 μm Si, one 500 μm Si, and four 6-cm-thick CsI detectors. The 50×50 mm^2 lateral dimensions of each telescope are divided into 256 square pixels ($\approx 3 \times 3$ mm^2), providing an angular resolution of about $\pm 0.43°$. The Si detectors are backed by four 6-cm-long CsI detectors. The center of the device was located at a polar angle of $\theta = 32°$ with respect to the beam axis, covering polar angles of $7° \leqslant \theta \leqslant 58°$. The array provided isotopic resolution $Z = 1$–8. This array provided excellent angular coverage for particles emitted in both peripheral and central collisions. Impact parameters were selected by assuming the multiplicity of charged particles, measured with LASSA [19,20] and the Miniball/Miniwall array [18] decrease monotonically with impact parameter; the combined apparatus covered 80% of the total solid angle.

Figure 2 shows the measured correlation between the charge of the projectile-like residue detected in the ring counter and the observed total charged particle multiplicity (measured in the Miniball/Miniwall and LASSA arrays). The projectile-like residue decreases monotonically in charge

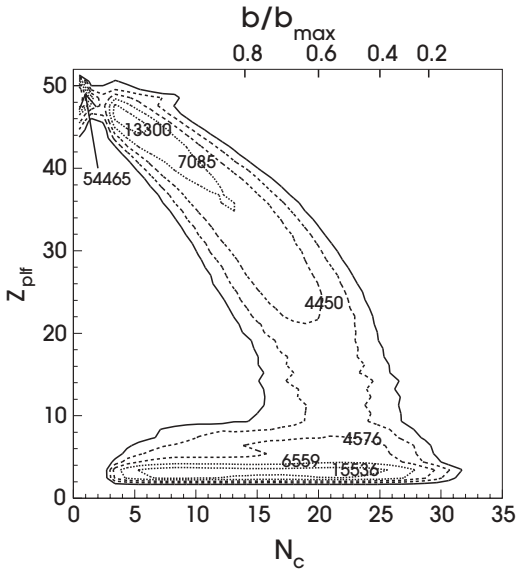

FIG. 2. Correlation between the charge of the projectile-like fragment ($Z_{\rm plf}$) and observed total charge particle multiplicity, N_C. The corresponding values of $b/b_{\rm max}$ are given in the upper axis of the figure. The numbers indicating the contour levels are in arbitrary units.

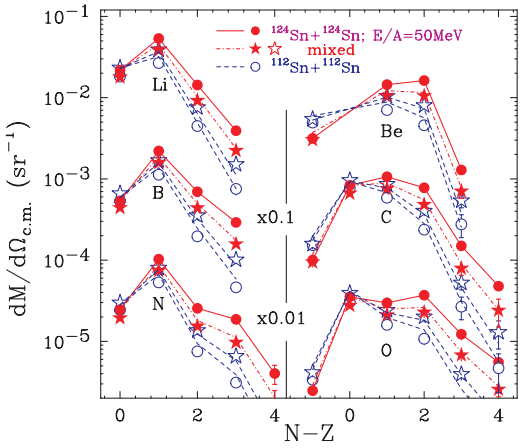

FIG. 3. (Color online) The solid circles, solid stars, open stars, and open circles show the experimental isotopic distributions at $y/y_{\rm beam} > 0.7$ and $b/b_{\rm max} > 0.8$ that has been measured for ^{124}Sn+^{124}Sn, ^{124}Sn+^{112}Sn, ^{112}Sn+^{124}Sn, and ^{112}Sn+^{112}Sn collisions, respectively. The solid lines are drawn to guide the eyes and the dashed lines are extrapolated from isoscaling parameters as discussed in the text.

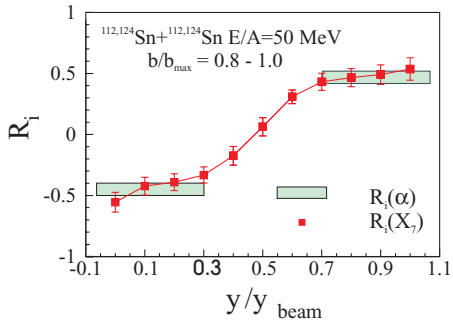

FIG. 4. (Color online) The shaded rectangles at $y/y_{\rm beam} < 0.3$ and $y/y_{\rm beam} > 0.7$ show the values of $R_i(\alpha)$ measured for the ^{124}Sn+^{112}Sn and ^{112}Sn+^{124}Sn systems, respectively [6]. The data points show the values of $R_i(X_7)$ measured for $A = 7$ mirror nuclei in peripheral ^{124}Sn+^{112}Sn collisions as a function of rapidity.

with decreasing impact parameter and appears to vanish at $b/b_{\rm max} \leqslant 0.4$. There is no evidence supporting the existence of a projectile-like residue in central collisions defined to be $b/b_{\rm max} < 0.2$. Isotopic distributions for midrapidity particles, which originate predominantly from the disintegration of the participant zone were measured with the gates $b/b_{\rm max} < 0.2$ and $70^\circ \leqslant \theta_{\rm c.m.} \leqslant 110^\circ$ and published in Ref. [13].

Figure 3 shows the isotopic distributions from peripheral collisions measured with impact parameter gate $b/b_{\rm max} > 0.8$ and projectile rapidity, $y/y_{\rm beam} > 0.7$ [6]. The solid lines are drawn through the data for the ^{124}Sn+^{124}Sn reaction. The other lines in the figure are extrapolated from the data measured for the ^{124}Sn+^{124}Sn reaction using Eq. (1) and the isoscaling parameters in Ref. [6]. These data and their isoscaling parameters were used in Ref. [6] to investigate the isospin diffusion. Values of $R_i(\alpha) = 0.47 \pm 0.05$ corresponding to the decay of the ^{124}Sn projectile from the ^{124}Sn+^{112}Sn reaction and $R_i(\alpha) = -0.45 \pm 0.05$ corresponding to the decay of the ^{112}Sn projectile from the ^{112}Sn+^{124}Sn reaction were obtained. These are shown by the shaded rectangles in Fig. 4; the ^{124}Sn projectile data are shown at $y/y_{\rm beam} > 0.7$ and ^{112}Sn projectile data are shown at $y/y_{\rm beam} < 0.3$ as the latter corresponds to the target in the ^{124}Sn+^{112}Sn reaction.

Now, we turn to the extraction of isospin transport ratios for the mirror nuclei. By combining the asymmetric collisions of ^{112}Sn+^{124}Sn and ^{124}Sn+^{112}Sn, we obtain complete coverage from projectile to target rapidity. The top two panels of Fig. 5 shows the background and efficiency corrected $d^2M/dyd(p_\perp/A)$ differential multiplicity distributions for ^{7}Li and ^{7}Be fragments for the ^{124}Sn+^{112}Sn reaction as a function of normalized rapidity $y/y_{\rm beam}$ and transverse momentum p_t/A. Here, both the particle rapidity and the beam rapidity are given in the laboratory frame. There is an angular cutoff in the experimental data at $\theta_{\rm lab} < 7^\circ$, corresponding to a rapidity dependent cut on the transverse momentum $p_\perp$. The projectile-like rapidity region near $y/y_{\rm beam} \sim 1$ is primarily obtained from the reaction ^{124}Sn+^{112}Sn using ^{124}Sn as the projectile, whereas the target-like rapidity region near $y/y_{\rm beam} \sim 0$ was transformed from the data of the inverse reaction, ^{112}Sn+^{124}Sn. Because ^{7}Li is a neutron-rich isotope, its yield is larger near the original rapidity ($y/y_{\rm beam} \sim 1$) of the neutron-rich ^{124}Sn projectile. The opposite is true for the proton-rich isotope, ^{7}Be, whose yield is larger near the original rapidity ($y/y_{\rm beam} \sim 0$) of the proton-rich ^{112}Sn target. For both fragments, the $d^2M/dyd(p_\perp/A)$ distributions are somewhat larger at midrapidity than at beam or target rapidity where the Coulomb repulsion between the fragments and the residue suppresses the fragment yield in a characteristic circular pattern about the rapidities of projectile- and targetlike residues.

One advantage of choosing isobars to study the isospin dependence of fragment formation is that the collective contribution to the energy is the same for both isobars; thus the relative admixture of thermal and collective energy contributions is the same for both. However, because the isobars have different charge, contributions from the Coulomb effect could be very large. The Coulomb effect is further amplified if the yield ratios of ^{7}Li and ^{7}Be are plotted as in the third panel of Fig. 5. This occurs because the Coulomb "circle" is larger for ^{7}Be than for ^{7}Li.

To disentangle the isospin effects from the Coulomb effects even in the midrapidity region, we construct the isospin transport ratio using Eq. (2). The nondiffusion effects of the Coulomb interaction should cancel to the first order. The bottom panel of Fig. 5 shows the 2D representation of the isospin transport ratios $R_7 = R_i\{\ln[Y(^7\text{Li})/Y(^7\text{Be})]\}$. By "normalizing" the observable $\ln[Y(^7\text{Li})/Y(^7\text{Be})]$ from the mixed systems with the two symmetric reactions, R_7 maximizes the effect of isospin diffusion. Comparing the bottom two panels, it is clear that effects from Coulomb force are largely canceled, even though it is difficult to be quantitative about cancellation in the regions, $y/y_{\rm beam} \sim 1$ and $y/y_{\rm beam} \sim 0$, at small transverse momenta where the Coulomb suppression makes the isotopic yields very small. The nearly complete elimination of the Coulomb effect demonstrates the power of the isotope transport ratio and suggests that other

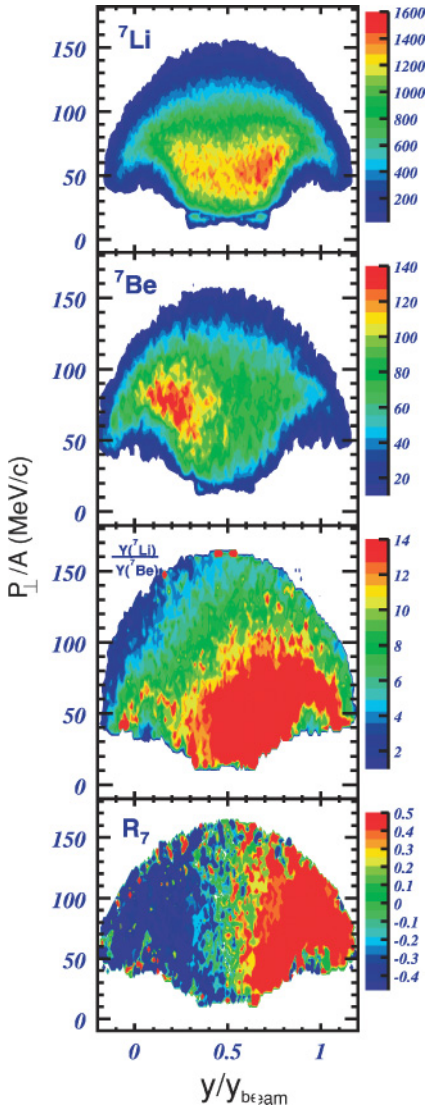

FIG. 5. (Color online) $d^2M/dyd(p_\perp/A)$ distribution as function of rapidity, $y/y_{\rm beam}$, measured in ^{124}Sn+^{112}Sn collisions at $E/A = 50$ MeV. From the top (first panel) ^{7}Li fragment distributions. (Second panel) ^{7}Be fragment distributions. (Third panel) Ratio of the ^{7}Li fragment distributions divided by the ^{7}Be distributions. (Fourth panel) R_7 distribution.

nondiffusion effects such as pre-equilibrium emissions are most likely largely canceled as well.

It is clear that R_7 makes a rapid transition through zero at midrapidity. It is nearly uniformly positive around the neutron-rich projectile rapidity and nearly uniformly negative around the neutron deficient target rapidity. The dependence on transverse momentum at a fixed rapidity is rather weak. The dependence on the rapidity as shown by the data points in Fig. 4 is obtained by integrating the transport isospin ratios R_7, over transverse momentum. R_7 is nearly flat near the projectile and the target rapidity regions before dropping to zero around midrapidity. As it can be seen from the comparison of the data points with the shaded boxes that depict the earlier isoscaling analyses, both analyses provide isospin transport ratios of about 0.47 ± 0.05 at $y/y_{\rm beam} = 0.7$–1.0 and -0.45 ± 0.05 at

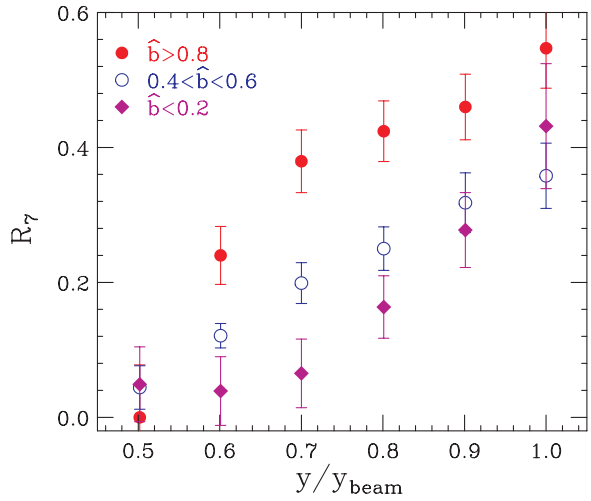

FIG. 6. (Color online) The solid diamonds, open circles, and solid circles show the rapidity dependencies of R_7 for central, midcentral, and peripheral collisions, respectively.

$y/y_{\rm beam} = 0$–0.3 when the same impact parameter and rapidity gates are applied to the same systems [6]. This suggests that the mirror nuclei ratios of mass 7 can be reliably used to assess the transport of isospin asymmetry throughout the collision.

Figure 6 shows the rapidity dependence of R_7 for $y/y_{\rm beam} > 0.5$ with three impact parameter gates: the peripheral gate ($b/b_{\rm max} > 0.8$) discussed earlier, a midimpact parameter gate ($0.4 < b/b_{\rm max} < 0.6$), and a central collision gate ($b/b_{\rm max} < 0.2$). To reduce the error bars, we have taken advantage of the approximate symmetry of R_7, i.e., $R_7(y/y_{\rm beam}) = -R_7(0.5 - y/y_{\rm beam})$ to combine results from both ^{124}Sn+^{112}Sn and ^{112}Sn+^{124}Sn collisions. The shape of R_7 changes significantly with impact parameter. For peripheral collisions, $b/b_{\rm max} > 0.8$, R_7 makes a rapid transition through zero near $y/y_{\rm beam} = 0.5$ and then remains roughly constant at $y/y_{\rm beam} > 0.8$. For midcentral collisions, $b/b_{\rm max} < 0.6$, R_7 changes linearly with rapidity. For central collisions, $b/b_{\rm max} < 0.2$, R_7 remains close to 0 for $0.5 < y/y_{\rm beam} < 0.7$ and then increases rapidly near projectile rapidity. At midrapidity and at projectile rapidity, within experimental uncertainties, R_7 seem to be independent of the impact parameter. R_7 decreases with impact parameters at rapidity between these two limits.

It appears that the isospin asymmetry in peripheral collisions makes a rapid transition between a value characteristic of target rapidity to another value characteristic of projectile rapidity. In central collisions, there is a broad domain near $y/y_{\rm beam} = 0.5$ where the values for R_7 ($R_7 \sim 0$) suggest isospin equilibrium and then a rapid transition to values ($R_7 \sim 0.5$) similar to that characteristic of peripheral collisions for $y/y_{\rm beam} \approx 1.0$. Such a trend is consistent with the picture that participant nucleons near $y/y_{\rm beam} = 0.5$ suffered collisions that mixed nucleons from the target and projectile nuclei nearly completely together. Mixing of nucleons near $y/y_{\rm beam} = 1.0$ is similar to the results observed in peripheral collisions. In an earlier study, Dempsey *et al.* [21] analyzed ratios of elemental and isotopic yields and observed significant nonequilibrium effects at both central and beam rapidities

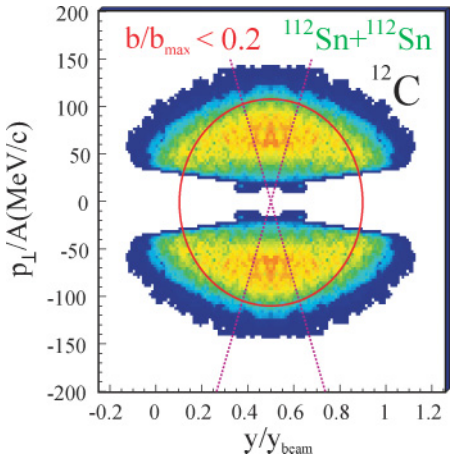

FIG. 7. (Color online) $d^2M/dyd(p_\perp/A)$ distribution for ^{12}C fragments produced in central ^{112}Sn+^{112}Sn collisions at $E/A = 50$ MeV. The dashed lines show the boundaries at $\theta_{c.m.} = 70^\circ$ and 110° for the mid-rapidity gate that was used to create the data shown in Fig. 1 [13]. The circle corresponds to the contour of constant velocity in the center of mass.

for ^{136,124}Xe+^{112,124}Sn collisions at $E/A = 55$ MeV. We are not able to compare directly those results to ours because the experimental observables and analyses techniques differ significantly. Additional measurements would be useful to establish more precisely the degree to which isospin equilibrium is achieved in central collisions.

The actual trajectories of nucleons that emerge near $y/y_{beam} = 1.0$ in central collisions are difficult to establish with the current data alone but may be addressed by detailed comparison with transport theory. Such comparisons lie outside the scope of the present article. One would like to address how many of these nucleons penetrate through the target and how many have trajectories that avoid the target. Similar trends are observed for the ^{11}C/^{11}B mirror nuclei ratios, albeit with significantly reduced statistics. Therefore it maybe useful to examine the emission pattern for ^{12}C fragments. Figure 7 shows the $d^2M/dyd(p_\perp/A)$ for ^{12}C fragments in central collisions. The circle corresponds to constant kinetic energy in the center-of-mass frame. Consistent with recent observations for ^{129}Xe+^{nat}Sn collisions [22], the measured momentum distributions are not spherical but are somewhat elongated along the beam axis. Because there are no projectile-like residues for these central collisions as it is shown in Fig. 2, this elongation is not caused by a projectile-like residue. In Ref. [22], such elongations were interpreted as a prolate deformation of a statistically equilibrated source. The present data suggest that the isospin equilibration of the source that emits fragments is not complete, and that a transparency could occur if the mean free path is comparable to the size of the system. If so, the present data may provide useful information about isospin dependent mean free path for nucleons in these collisions.

In summary, we have demonstrated that the ratios of the yields of mirror nuclei, such as $Y(^7\mathrm{Li})/Y(^7\mathrm{Be})$, can be an effective observable for studying the isospin diffusion phenomenon. Such ratios have the virtue of being less sensitive to the unknown admixtures of collective and thermal motion. We also demonstrated that the isospin transport ratios remove the distortions due to effects such as Coulomb repulsion that could obscure the effects of the density dependence of the symmetry energy. Similar trends are observed for R_{11} constructed from the $Y(^{11}\mathrm{B})/Y(^{11}\mathrm{C})$ ratio. (The other mirror nuclei pair constructed from $Y(^3\mathrm{H})/Y(^3\mathrm{He})$ does not appear to be as suitable for the diffusion studies because the pre-equilibrium contributions and thermal momentum contributions are much larger.) Statistical theories predict observables such as α, β, or X_A depend linearly on the isospin asymmetry δ. In such circumstances, the isospin transport ratios corresponding to these observables should be equal to those constructed from the isospin asymmetry δ of the source at the time when the particles are emitted. This is confirmed by our central collisions data.

We have explored the impact parameter and rapidity dependence of the isospin transport ratios, and of the local isospin asymmetry itself. We find that the isospin transport ratios for ^{112,124}Sn+^{112,124}Sn collisions increase monotonically with rapidity. The transition from negative ratios at proton-rich target rapidity to positive ratios at neutron-rich projectile rapidity changes with impact parameter. For large impact parameters, the change at midrapidity is abrupt and there is a large region of roughly constant isospin asymmetry ratio near beam and target rapidity. As the impact parameter decreases, this transition becomes more gradual. For central collisions, there is a large region around midrapidity with small isospin transport ratios, consistent with isospin equilibrium.

ACKNOWLEDGMENTS

This work is supported by the National Science Foundation under grant numbers PHY-0110253, PHY-0606007(MSU) and by the DOE under grant numbers DE-FG02-87ER-40316 (WU) and DE-FG02-88ER-40404 (IU).

[1] P. Danielewicz, R. Lacey, and W. Lynch, Science **298**, 1592 (2002), and references therein.
[2] J. Lattimer and M. Prakash, Astrophys. J. **550**, 426 (2001).
[3] B. A. Brown, Phys. Rev. Lett. **85**, 5296 (2000).
[4] C. J. Horowitz, S. J. Pollock, P. A. Souder, and R. Michaels, Phys. Rev. C **63**, 025501 (2001).
[5] B.-A. Li, Phys. Rev. Lett. **85**, 4221 (2000).
[6] M. B. Tsang, T. X. Liu, L. Shi, P. Danielewicz, C. K. Gelbke, X. D. Liu, W. G. Lynch, W. P. Tan, G. Verde, A. Wagner *et al.*, Phys. Rev. Lett. **92**, 062701 (2004).
[7] L. Shi and P. Danielewicz, Phys. Rev. C **68**, 064604 (2003).
[8] L.-W. Chen, C. M. Ko, and B.-A. Li, Phys. Rev. Lett. **94**, 032701 (2005).
[9] F. Rami, Y. Leifels, B. de Schauenburg, A. Gobbi, B. Hong, J. P. Alard, A. Andronic, R. Averbeck, V. Barret, Z. Basrak *et al.*, Phys. Rev. Lett. **84**, 1120 (2000).

[10] M. B. Tsang, W. A. Friedman, C. K. Gelbke, W. G. Lynch, G. Verde, and H. S. Xu, Phys. Rev. Lett. **86**, 5023 (2001).
[11] A. S. Botvina, O. V. Lozhkin, and W. Trautmann, Phys. Rev. C **65**, 044610 (2002).
[12] A. Ono, P. Danielewicz, W. A. Friedman, W. G. Lynch, and M. B. Tsang, Phys. Rev. C **68**, 051601(R) (2003).
[13] T. X. Liu, M. J. van Goethem, X. D. Liu, W. G. Lynch, R. Shomin, W. P. Tan, M. B. Tsang, G. Verde, A. Wagner, H. F. Xi *et al*., Phys. Rev. C **69**, 014603 (2004).
[14] M. B. Tsang, C. K. Gelbke, X. D. Liu, W. G. Lynch, W. P. Tan, G. Verde, H. S. Xu, W. A. Friedman, R. Donangelo, S. R. Souza *et al*., Phys. Rev. C **64**, 054615 (2001).
[15] W. P. Tan, S. R. Souza, R. J. Charity, R. Donangelo, W. G. Lynch, and M. B. Tsang, Phys. Rev. C **68**, 034609 (2003).
[16] H. S. Xu, M. B. Tsang, T. X. Liu, X. D. Liu, W. G. Lynch, W. P. Tan, A. V. Molen, G. Verde, A. Wagner, H. F. Xi *et al*., Phys. Rev. Lett. **85**, 716 (2000).
[17] T. X. Liu, W. G. Lynch, M. J. van Goethem, X. D. Liu, R. Shomin, W. P. Tan, M. B. Tsang, G. Verde, A. Wagner, H. F. Xi *et al*., Europhys. Lett. **74**, 806 (2006).
[18] R. DeSouza, N. Carlin, Y. Kim, J. Ottarson, L. Phair, D. Bowman, C. Gelbke, W. Gong, W. Lynch, R. Pelak *et al*., Nucl. Instrum. Methods A **295**, 109 (1990).
[19] A. Wagner, W. Tan, K. Chalut, R. Charity, B. Davin, Y. Larochelle, M. Lennek, T. Liu, X. Liu, W. Lynch *et al*., Nucl. Instrum. Methods Phys. Res., Sect. A **456**, 290 (2001).
[20] B. Davin, R. de Souza, R. Yanez, Y. Larochelle, R. Alfaro, H. Xu, A. Alexander, K. Bastin, L. Beaulieu, J. Dorsett *et al*., Nucl. Instrum. Methods A **473**, 302 (2001).
[21] J. F. Dempsey, R. Charity, L. Sobotka, G. Kunde, S. Gaff, C. Gelbke, T. Glasmacher, M. Huang, R. Lemmon, W. Lynch *et al*., Phys. Rev. C **54**, 1710 (1996).
[22] A. L. Fèvre, M. Płoszajczak, V. Toneev, G. Auger, M. L. Begemann-Blaich, N. Bellaize, R. Bittiger, F. Bocage, B. Borderie, R. Bougault *et al*., Nucl. Phys. **A735**, 219 (2004).